JGR Oceans

RESEARCH ARTICLE
10.1029/2020JC016605

Key Points:
- Radium-derived mixing rates varied between 3,236 and 467 $m^2\ s^{-1}$ as a function of river discharge rates and shelf geometry
- 2.3×10^{10}–4.5×10^9 mol C d^{-1} in the form of DIC is exported across the shallow region of the shelf during high and low river flow seasons
- The Louisiana shelf represents a major source of DIC to the GOM

Supporting Information:
- Supporting Information S1

Correspondence to:
K. Maiti,
kmaiti@lsu.edu

Citation:
Anderson, M. M., Maiti, K., Xue, Z. G., & Ou, Y. (2020). Dissolved inorganic carbon transport in the surface-mixed layer of the Louisiana Shelf in northern Gulf of Mexico. *Journal of Geophysical Research: Oceans*, *125*, e2020JC016605. https://doi.org/10.1029/2020JC016605

Received 22 JUL 2020
Accepted 19 OCT 2020
Accepted article online 26 OCT 2020

Dissolved Inorganic Carbon Transport in the Surface-Mixed Layer of the Louisiana Shelf in Northern Gulf of Mexico

M. M. Anderson[1], K. Maiti[1,2], Z. George Xue[1,2,3], and Y. Ou[1]

[1]Department of Oceanography and Coastal Sciences, Louisiana State University, LA, Baton Rouge, USA, [2]Coastal Studies Institute, Louisiana State University, Baton Rouge, LA, USA, [3]Center for Computation and Technology, Louisiana State University, Baton Rouge, LA, USA

Abstract Rivers and wetlands are a major source of terrestrial derived carbon for coastal ocean margins. This results in a net loss of terrestrial carbon into the shelf water and their subsequent transport to interior ocean basin. This study investigates the transport of dissolved inorganic carbon (DIC) in the surface-mixed layer of Louisiana Shelf in northern Gulf of Mexico (nGOM) adjacent to the Wax Lake Delta (WLD) and Barataria Bay (BB), which represent contrasting net land gain and net land loss areas in this region. DIC samples were collected, in conjunction with short-lived radium isotopes ^{224}Ra ($t_{1/2}$ = 3.66 days) and ^{223}Ra ($t_{1/2}$ = 11.43 days) samples during June and September 2019, to quantify shelf transport of DIC in the surface-mixed layer during period of high and low river flow, respectively. Radium distribution implied shelf mixing rates of 140–6,759 and 63–2,724 $m^2\ s^{-1}$ for WLD and BB regions, respectively, with more than tenfold decrease in rates between the two seasons. Net shelf transport of DIC was found to be highest for the WLD region in June, highlighting the importance of freshwater discharge in exporting DIC. An upscaling of our study for the entire Louisiana Shelf indicates that 1.54–20.19×10^9 mol C d^{-1} transported in June 2019 and 0.34–8.12×10^9 mol C d^{-1} in the form of DIC was exported across the shallow region of the shelf during high and low river flow seasons, representing an important source of DIC to the NGOM.

Plain Language Summary Rivers and wetlands are a major source of terrestrial derived carbon for coastal ocean margins. This results in a net loss of terrestrial carbon into the shelf water and their subsequent transport to interior ocean basin, which are currently not well constrained. In the current study, we used naturally occurring short-lived radium radioisotopes to understand the transport of dissolved inorganic carbon across the Louisiana Shelf in northern Gulf of Mexico. This region receives a large amount of dissolved carbon from the Mississippi-Atchafalaya River System as well as coastal wetland loss, but the fate and transport of this carbon is not well documented. Our study indicates that the DIC transport across the Louisiana Shelf can vary from 0.02–0.24 to 0.03–0.09 Tg C d^{-1} during high and low river flow seasons, representing an important source of DIC to the Gulf of Mexico that is predominately controlled by river discharge. Current predictions suggest that Mississippi-Atchafalaya River discharge to coastal waters may increase by up to 60% by 2090, which would have dramatic impact on the lateral export of both carbon and nutrients to the ocean interior in the future.

1. Introduction

Deltaic systems are a major pathway for the input of terrestrial derived carbon to the coastal ocean (Bianchi et al., 2004, 2007). Globally, rivers and associated coastal wetlands transport approximately 1.0 Gt carbon from continental regions to oceans annually (Cai et al., 2015; Suchet et al., 2003). Dissolved inorganic carbon (DIC), which is the sum of all carbonate species dissolved in water (DIC = $[HCO_3^-] + [CO_3^{-2}] + [CO_2]$) represents about 41% of this transported carbon (Cai et al., 2015; Suchet et al., 2003). Despite the importance of these systems, there is still a lack of understanding about the interaction and temporal-spatial linkages between highly productive wetlands and the adjacent coastal waters in terms of a carbon budget (Bianchi et al., 2004, 2007; Hopkinson et al., 2012). The need for a comprehensive understanding of the transport of carbon to the coastal ocean is made even more imperative, as global coastal wetlands are undergoing substantial alterations due to climatic and anthropogenic forcing.

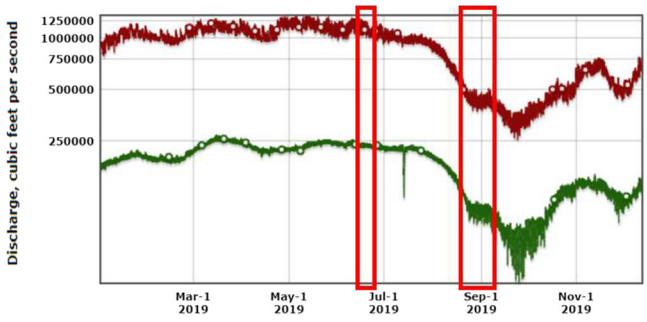

Figure 1. Freshwater discharge rates during 2019 for the Mississippi River at Belle Chase, LA (USGS 07374525, red line) and Wax Lake Outlet at Calumet, LA (USGS 07381590, green line). The vertical rectangles indicate sampling period.

It is estimated that global coastal wetland coverage could be reduced between 30% and 59% by the end of this current century, based on current sea level rise and levels of human intervention (Schuerch et al., 2018; Spencer et al., 2016). Nowhere is this more apparent than the Mississippi River (MSR) Delta in the northern Gulf of Mexico (nGOM). This is the largest deltaic system in the region, accounting for 40% of the wetlands within the conterminous United States (Bi et al., 2019; Bianchi et al., 2011). Currently, coastal Louisiana is experiencing relative sea level rise at rates faster than most coastlines around the world (Kolker et al., 2011). While eustatic sea level rise is estimated to range between 3 and 4 mm yr^{-1} (Intergovernmental Panel on Climate Change, 2014), some areas of the Louisiana coast are subsiding at 6–8 mm yr^{-1} as a result of reduced sediment supply to the wetlands, associated with upstream dams and the extensive levee infrastructure along the MSR (Blum & Roberts, 2009). The high rates of erosion and deterioration result in the rapid loss of 26–30 km^2 of wetlands per year from this region, thereby generating a net loss of carbon, which would otherwise be stored in the wetlands (Barras, 2006; Couvillion, 2011; Couvillion et al., 2017). While the wetland loss in this region is well documented, the associated carbon being transported into and across the continental shelf is not well constrained.

The exchange of material between the eroding continental margin and ocean interior plays a major role in global biogeochemical cycles. However, material fluxes across shelf waters are difficult to quantify, as these systems are exceedingly complex due to small-scale temporal and spatial variability. Commonly, freshwater plumes and their dissolved materials are traced by offshore negative salinity and/or positive silica anomalies (Chen et al., 2010). However, the salinity signal can be altered by evaporation and precipitation, and the silica signal is sensitive to biological uptake (Chen et al., 2010). To avoid some of these drawbacks, naturally occurring short-lived radium isotopes (^{224}Ra and ^{223}Ra) have been successfully utilized to quantify fluxes of dissolved components transported across continental shelves (Burt et al., 2013; Li & Cai, 2011; Moore & Krest, 2004; Sippo et al., 2019; Windom et al., 2006).

In this study, we evaluate the lateral transport of DIC in the surface-mixed layer using ^{224}Ra ($t_{1/2}$ = 3.6 days) and ^{223}Ra ($t_{1/2}$ = 11.43 days) across two sections of the Louisiana Shelf with contrasting rates of land loss and organic matter:mineral content. The Wax Lake Delta (WLD) is one of the few regions in Louisiana undergoing sediment accretion, due to large inputs of mineral sediment through the Wax Lake Outlet, an artificial channel off the Atchafalaya River (AR) (Rosen & Xu, 2013). The outlet was built by the U.S. Army Corps of Engineers in 1941 to protect Morgan City, Louisiana during high flood stages by diverting 30% of the AR flow to the nGOM (Rosen & Xu, 2013; Second New Orleans District, U.S. Army Corps of Engineers, 1938). In contrast to WLD, the Barataria Bay (BB) region has historically high land loss rates, due to the lack of mineral sediment input, preventing the land from keeping up with sea level rise and subsidence (Barras et al., 2003; Blum & Roberts, 2009). We thus hypothesize that (i) larger freshwater outflow into the shallow shelf of the WLD region will result in a larger oceanward transport of DIC compared to the BB region and (ii) the magnitude of DIC transport will be higher in late spring (June) than in late summer (September), due to the seasonal decrease in river discharge.

2. Materials and Methods

2.1. Study Site

The WLD region represents an area of net wetland gain in Louisiana (Figure 1). WLD was recently formed as a result of dredging efforts that diverted water from AR to the nGOM, moving sediment input through the man-made Wax Lake Outlet (Rosen & Xu, 2013). Formation of WLD began in 1972, with accelerated growth occurring after large scale floods during the years of 1973–1975 (Rosen & Xu, 2013). Since these events, the delta has been growing naturally, with minimal active management (Allen et al., 2012). The delta's current extension is 65 km^2, accreting land at a rate of 1 km^2 yr^{-1} (Allen et al., 2012). This growth rate has allowed for the establishment of marsh and forested wetland vegetation across elevation gradients (Holm & Sasser, 2001). The WLD is less than 14 km from the mouth of the AR, where both of the AR and Wax Lake Outlet discharge directly into the Atchafalaya Bay before entering the nGOM.

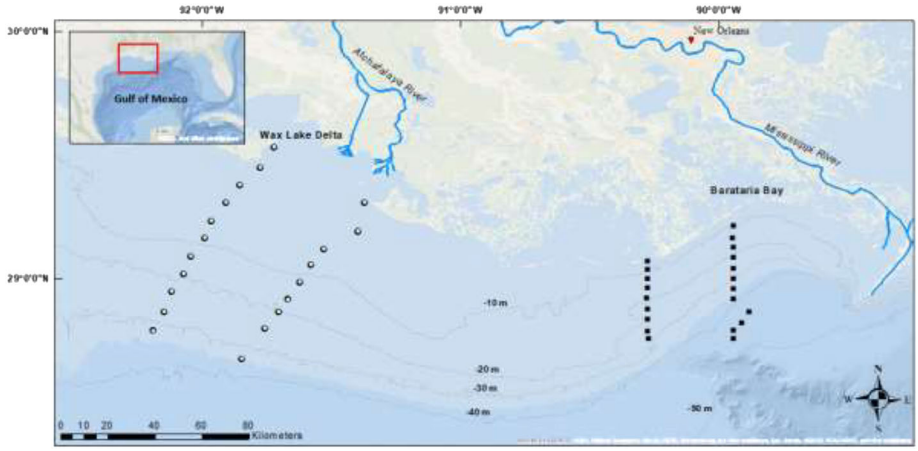

Figure 2. Map of the study area showing sampling locations in the Wax Lake Delta sector (left) and the Barataria Bay sector (right).

In contrast to WLD, the BB has historically experienced significant wetland loss. The Barataria Basin occupies more than 6,000 km^2 of wetlands and bodies of water (FitzGerald et al., 2004). The basin is bordered by the abandoned Bayou Lafourche distributary to the west, the mainstem of the active MSR to the east and a series of barrier islands to the south, separating the estuary from the nGOM (FitzGerald et al., 2004). The basin is currently experiencing extensive loss of wetlands, with an estimated loss of 23 km^2 yr^{-1} (Barras, 2006; Couvillion, 2011; Couvillion et al., 2017) and a loss of soil organic carbon of 1,000–2,050 g C m^{-2} yr^{-1} (Wang et al., 2017). Subsidence and wetland loss in BB are predicted to continue and increase drastically, due to a coupling of increasing sea level rise and decreased modern sediment loading to the deltaic plain (Barras et al., 2003; Blum & Roberts, 2009).

WLD and BB thus represent two extremes of the ongoing changes to the Louisiana coast, in which both wetland/deltaic systems are in constant flux with the nGOM. Both regions produce freshwater plumes, providing an important source of DIC to shelf waters as they mix (Cai et al., 2011; Suchet et al., 2003). Yet, despite the importance of these coastal ecosystems, there is still a lack of understanding about the temporal and spatial linkages between the coastal wetlands, adjacent shelf waters, and their carbon transport through mixing. One major temporal shift in southeast Louisiana can be the seasonal decrease of river discharge, which was quite dramatic in 2019 (Figure 1). In 2019, the river discharge was high (125×10^4 and 25×10^4 ft^3 s^{-1} for the MSR and Wax Lake Outlet) during late spring and early summer as a result of freshwater input from snowmelt in the northern United States (Figure 1). However, by early September, the freshwater discharge is reduced to 45×10^4 and 10×10^4 ft^3 s^{-1} for the MSR and Wax Lake Outlet, respectively. Thus, our seasonal sampling during June and September of 2019, shown in boxes in Figure 1, can provide a better understanding of how such drastic decreases in freshwater can alter the DIC transport in coastal shelf waters.

2.2. Stations and Cruises

Field sampling was conducted on the *R/V* Acadiana during June 2019 and September 2019 to account for seasonal high and low river discharges of the MSR, AR, and Wax Lake Outlet (Figure 2). The samples were collected along two cross-shelf transects for both the WLD and BB regions, referred to as West and East (Figure 2). Surface water sampling was collected from 1 m below the surface at 9-km intervals for WLD transects and 5-km intervals for BB transects, until a salinity of ~30 was reached in June 2019. These stations were repeated in September 2019 (Figure 2). The WLD sector extended 84 km offshore, and the BB sector extended 57 km offshore, to reach a water depth of at least 35 m.

2.3. Sample Collection and Analysis

Radium water samples were collected in cubitainers by filtering 60-L water through a 1.0-μm cartridge filter. The filtered water sample was immediately drained through a column containing 20 g of manganese oxide coated fibers (Mn-fiber) at a rate of <1 L min^{-1} to quantitatively collect radium as described by

Moore (1976). In the laboratory, each Mn-fiber sample was rinsed with radium free water with a pH of 7, partially dried in the open air or by a stream of dry air and then measured for ^{224}Ra and ^{223}Ra using a delayed-coincidence system as described by Moore and Arnold (1996).

For DIC samples, water was passed through a 0.45-mm glass fiber syringe filter and collected into Labco septa vials (https://www.labco.uk) in duplicates thoroughly flushed with extensive overflow and spiked with a 5-μl saturated $HgCl_2$ solution. DIC samples were stored at 5°C and measured back in the laboratory within a week of collection, using the standard protocol for the semi-automated system Apollo SciTech DIC Analyzer. The Apollo SciTech DIC Analyzer was calibrated using certified reference materials (CRM batch 180; Dickson, 2010).

2.4. Calculation of Mixing Coefficients

Radium isotopes have been used by a number of previous studies to measure coastal mixing rates across continental shelves, including the South Atlantic Bight, southern Brazil, the South China Sea, the Scotian Shelf, and the Gulf of Carpentaria (Burt et al., 2013; Chen et al., 2010; Moore, 2000; Sippo et al., 2019; Windom et al., 2006). There are four natural isotopes of radium produced from natural uranium and thorium decay. This work utilizes ^{224}Ra and ^{223}Ra, which have short half-lives of 3.66 and 11.4 days, respectively. These isotopes are introduced to seawater through contact with thorium-bearing sediments carried by fresh river water or deposited bottom sediments (Chen et al., 2010; Moore & Krest, 2004). Radium isotopes are strongly adsorbed on sediments in fresh river water and will desorb as they come in contact with the high ionic strength of coastal waters (Chen et al., 2010; Moore & Krest, 2004). Once introduced to near shore waters, the radium's activity can only decrease by mixing with water with a lower activity and by radioactive decay (Chen et al., 2010; Moore & Krest, 2004). Since the short-lived radium isotopes decay rapidly, their activities will quickly decrease with increasing distance from their fresh water source (Chen et al., 2010). By tracking the decay of these two short-lived radium isotopes, the time scale of transport of freshwater as it moves across the shelf and mixes with adjacent coastal waters can be constrained (Chen et al., 2010; Moore, 2000; Moore & Krest, 2004; Windom et al., 2006). The distribution of these short-lived isotopes over the shelf can be modeled and cross-shelf mixing rates determined using the following equation (Moore, 2000).

$$\ln A_x = \ln A_0 - x(\lambda/K_h)^{1/2} \quad (1)$$

where A_x is the measured activity at distance x from shore, A_0 is the activity at the shoreline, K_h is the mixing coefficient, and λ is the decay constant. Several assumptions are required to apply this model: (1) radium addition to the surface water occurs only in the near-shore zone; (2) net cross-shelf advection is negligible compared to mixing; (3) cross-shelf mixing is constant throughout the respective sampling period; (4) the system is in steady state (Moore, 2000). In this study, we utilize short-lived ^{224}Ra and ^{223}Ra, as their concentration in the open ocean can be assumed to be negligible. Bottom sediments can be an important source of Ra to the overlying water column. However, during both the study periods, strong water column stratification was observed based on salinity (referred to in the next section), suggesting negligible input from sediments. The largest source of uncertainty is associated with mixing rates (K_h) calculated from the radium distribution over distance curve fitting in Equation 1. Throughout this manuscript, uncertainties associated with K_h and other parameters derived from K_h are calculated using regression analysis and expressed as a range representing the upper and lower 90% confidence interval.

3. Results

3.1. Wind and Salinity Distribution

In WLD transects, during June 2019, average wind direction was oriented to the west and average wind speed was 4.7 m s^{-1} (National Data Buoy Center, 1971). Surface salinity (S) increased from 2 to 30 with distance from shore. There was a strong vertical stratification at around 5-m depth, separating the upper mixed layer and bottom water (Figure 3). During September 2019, average wind direction was oriented to the north, average speed was 3.93 m s^{-1} (National Data Buoy Center, 1971), and surface S increased from 4 to 29 with distance from shore and showed vertical stratification at around 8-m depth (Figure 3). The

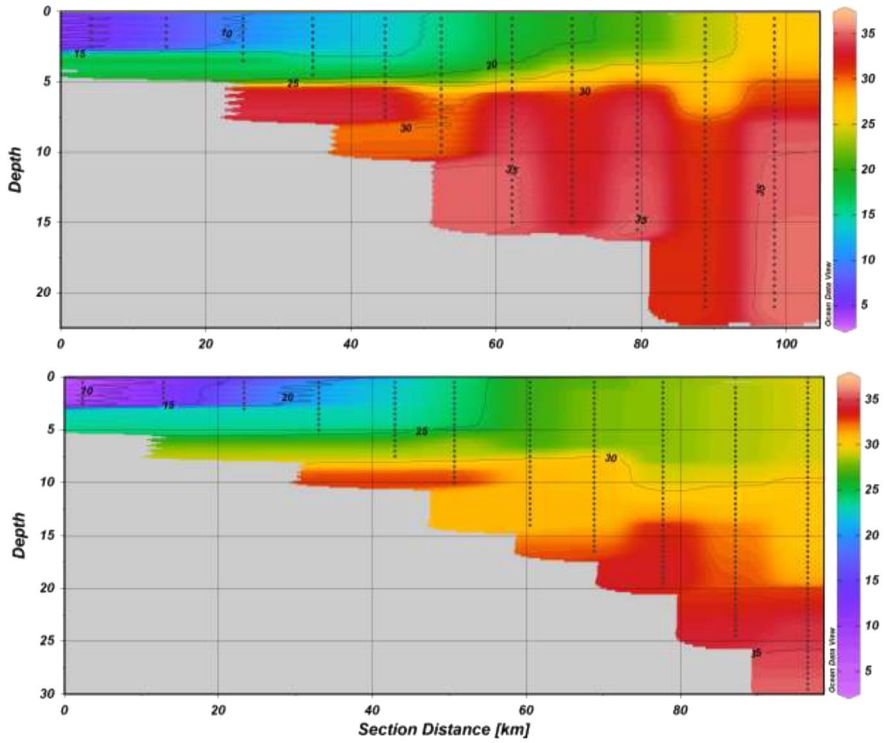

Figure 3. Salinity distribution along the WLD sector during June 2019 (top panel) and September 2019 (bottom panel).

prominent surface freshwater lens observed in June 2019 was less pronounced by September 2019, due to reduced freshwater input in the shelf.

For the BB transects, during June 2019, average wind direction was oriented to the north northeast, with an average wind speed of 2.4 m s^{-1} (National Data Buoy Center, 1971). The surface *S* increased from 13 to 27 with distance offshore. There was a strong vertical stratification at around 5- to 7-m depth, separating the upper mixed layer and bottom water (Figure 4). In September 2019, the *S* was significantly different from June 2019 (*t* test, $P < 0.05$), with a much higher *S* being observed, varying from 23 to 30. A vertical stratification at around 7-m depth was still present (Figure 4). The average wind direction was oriented to the northwest and average wind speed was 2.54 m s^{-1} (National Data Buoy Center, 1971).

3.2. DIC Distribution

In June 2019, the surface DIC concentration in both the WLD transects ranged between 1,765 and 2,290 μmol kg^{-1}, with a mean concentration of 1,979 ± 103 μmol kg^{-1}. In September 2019, the DIC concentrations ranged between 1,721 and 2,153 μmol kg^{-1}, with a mean concentration of 1,924 ± 90 μmol kg^{-1} (Table 1). There was no significant trend with distance offshore.

For both BB transects, DIC concentrations ranged between 1,926 and 2,279 μmol kg^{-1}, with a mean concentration of 2,043 ± 72 μmol kg^{-1} in June 2019, while in September 2019, the DIC ranged from 1,851 to 2,390 μmol kg^{-1}, with a mean concentration of 2,047 ± 132 μmol kg^{-1} (Table 1). Similar to WLD, there was no significant trend with season or distance offshore.

3.3. ^{224}Ra and ^{223}Ra Distribution

In June 2019, the distribution of ^{224}Ra and ^{223}Ra ranged from 68 to 4 dpm 100 L^{-1} and from 9 to 0.9 dpm 100 L^{-1} (Figures 5 and 6). By September 2019, the activities of both ^{224}Ra and ^{223}Ra in the WLD transects were found to be significantly different from the activities in June 2019 (*t* test, $P < 0.05$), as the distribution of ^{224}Ra and ^{223}Ra now ranged from 19 to 0.05 dpm 100 L^{-1} and from 2 to 0.05 dpm 100 L^{-1} (Figures 5 and 6). Thus, between June 2019 and September 2019, the distribution range and mean activity of ^{224}Ra

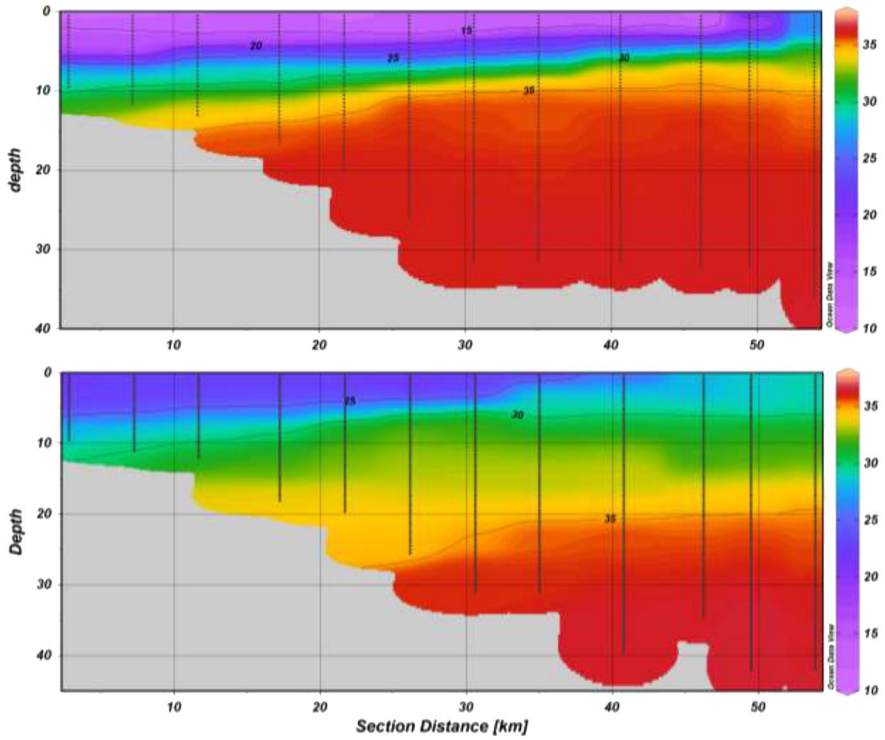

Figure 4. Salinity distribution along the BB sector during June 2019 (top panel) and September 2019 (bottom panel).

decreased by 45 dpm 100 L^{-1}, while the distribution range of ^{223}Ra decreased by 6 dpm 100 L^{-1}. During both seasons, the WLD transects experienced a decrease of ^{224}Ra and ^{223}Ra activities with distance offshore.

The distribution of ^{224}Ra and ^{223}Ra activities in the BB transects decreased offshore in both seasons. In June 2019, the distribution of ^{224}Ra and ^{223}Ra ranged from 54 to 2 dpm 100 L^{-1} and from 7 to 1 dpm 100 L^{-1}, (Figures 7 and 8). In September 2019, the distribution of ^{224}Ra and ^{223}Ra ranged from 11 to 0.4 dpm 100 L^{-1} and from 1 to 0.09 dpm 100 L^{-1} (Figures 7 and 8). Overall, the distribution range of ^{224}Ra decreased by 41 dpm 100 L^{-1}, while that of ^{223}Ra decreased by 5 dpm 100 L^{-1}, respectively, representing a significant difference in the distribution between the two seasons (t test, $P < 0.05$).

In summary, both ^{223}Ra and ^{224}Ra activities in the WLD and BB sectors decreased with distance from shore, although some nearshore stations within ~1 km from coast showed low activities. We attribute these lower activities to incomplete desorption of radium from sediments because of the low salinity at these stations. When low-salinity river water mixes with seawater, radium is rapidly desorbed from suspended particles, and this process is essentially complete at salinity of about 5 (Krest et al., 1999). The log-linear distribution of ^{224}Ra and ^{223}Ra activities across all transects suggests cross-shelf mixing plays an important role in offshore transport of ^{224}Ra and ^{223}Ra, with minimal impact from benthic fluxes (Moore, 2000; Sippo et al., 2019). Sediment core incubations carried out in this region between 2016 and 2019 showed benthic diffusive fluxes of ^{224}Ra and ^{223}Ra represent less than 6% of the water column's radium inventories (Bam et al., 2016).

Table 1
^{224}Ra- and ^{223}Ra-Based Estimates of Mixing Rates and Residence Time for WLD and BB

Sector	Month	K_h ^{224}Ra (m^2 s^{-1})	K_h ^{223}Ra (m^2 s^{-1})	Residence time ^{224}Ra (days)	Residence time ^{223}Ra (days)	Average DIC (μmol kg^{-1})
Wax Lake Delta	June	1,284–5,491	478–6,759	71–118	99–311	1,979 ± 103
	September	241–699	140–1,610	58–170	25–291	1,924 ± 90
Barataria Bay	June	497–2,373	458–2,724	93–140	58–151	2,043 ± 72
	September	124–1,148	63–1,228	16–151	15–300	2,047 ± 132

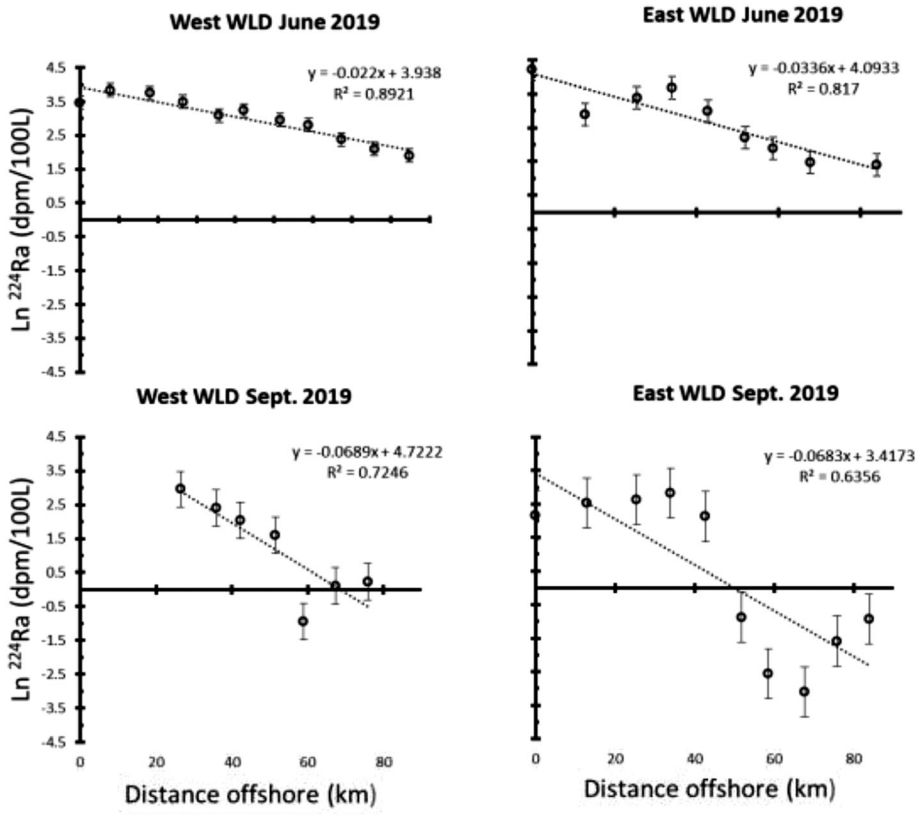

Figure 5. ^{224}Ra distribution along the two transects in Wax Lake Delta (WLD) during June 2019 (upper panels) and September 2019 (lower panels).

4. Discussion

The ^{224}Ra and ^{223}Ra activities found in this study ranged from 68 to 0.05 dpm 100 L^{-1} and from 11 to 0.05 dpm 100 L^{-1}, which are similar to previous reported activities between 43.5 to −0.3 dpm 100 L^{-1} and 3.78–0.04 dpm 100 L^{-1} from sampling in 1994 in the Louisiana Shelf (Moore & Krest, 2004). The mixing rates along each cross-shelf transect of the WLD and BB sectors were determined from log-linear radium distributions with distance (Figure 9), all of which showed significant (P value < 0.01) linear correlation. There is a large variability in mixing rates for transects within the same sector, which we attribute to spatial heterogeneity and differences in physical processes within each region. The mixing rates calculated independently from the ^{224}Ra and ^{223}Ra distribution show similar rates along most transects and the differences in rates derived from each isotope is probably due to the differences in their half-lives of 3.66 and 11.4 days, respectively (Moore, 2000).

4.1. Radium-Derived Mixing Rates

Mixing rates (K_h) were estimated from the distribution of ^{224}Ra and ^{223}Ra activities with distance from shore using (Equation 1) for each of the eight transects (Figure 9). For the rest of the discussion, we report the average value of the west and east transects for the WLD and BB sectors to represent the average mixing rates within these regions (Table 1). In June 2019, the WLD had mixing rate ranging between 1,284–5,491 and 478–6,759 m^2 s^{-1} for ^{224}Ra and ^{223}Ra, respectively, while the BB transects had mixing rates ranging between 497–2,373 and 458–2,724 m^2 s^{-1} for ^{224}Ra and ^{223}Ra, respectively (Figure 9). In September 2019, the WLD transects had mixing rates ranging from 241 to 699 and from 140 to 1,610 m^2 s^{-1} for ^{224}Ra and ^{223}Ra, respectively (Figure 9) The BB transects had average mixing rates ranging from 124 to 1,148 and 63 to 1,228 m^2 s^{-1} for ^{224}Ra and ^{223}Ra (Figure 9). The WLD region experienced up to 8 times decrease in average mixing rates between June 2019 and September 2019, while the BB transects experienced up to 4 times decrease in average mixing rates (Table 1).

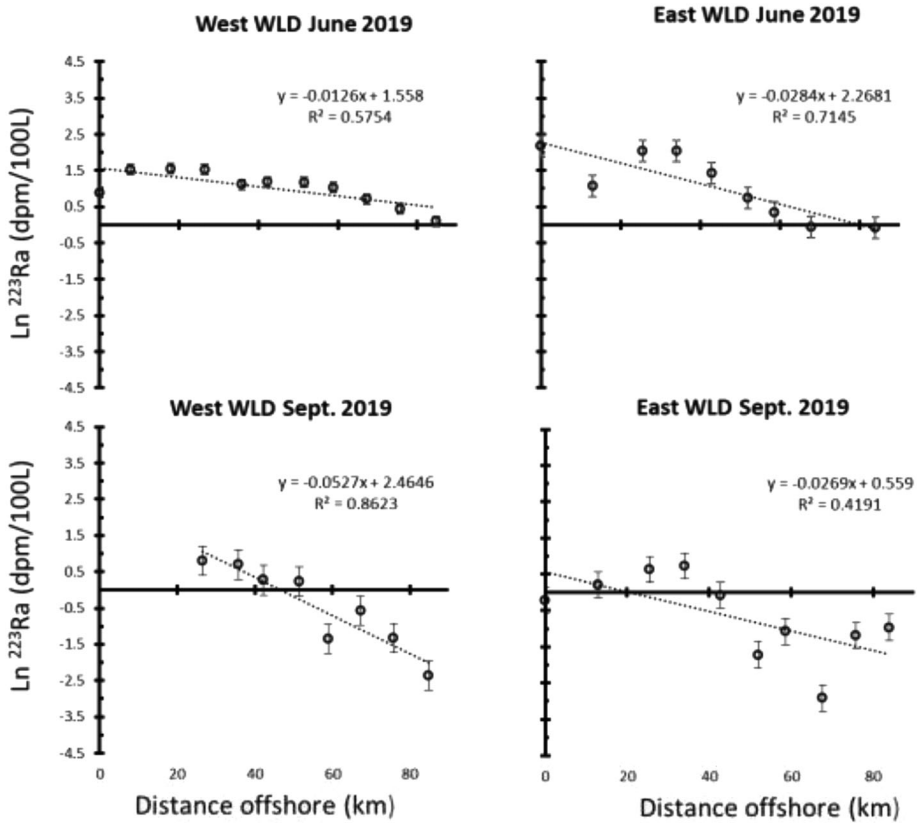

Figure 6. ^{223}Ra distribution along the two transects in Wax Lake Delta (WLD) during June 2019 (upper panels) and September 2019 (lower panels).

The decrease in mixing rates between June and September can be attributed to the observed decrease in seasonal river discharge during this timeframe (Figure 1). While both the WLD and BB regions experienced a decrease in mixing rates as freshwater discharge decreased, this does not explain the difference between the two sectors within the same season. The differences in average K_h estimates for WLD and BB during each season could be due to the fact that the Wax Lake Outlet and AR discharge directly into the shallow shelf region of the WLD sector, As the river water pools on the shallow shelf in the Wax Lake and Atchafalaya Region, instabilities along the plume edge can then result in turbulent flow and a net offshore transport of the plume water (Thyng & Hetland, 2018). Previous studies of seasonal freshwater transport on the Louisiana Shelf, using hydrodynamic models and Lagrangian trajectory models, concluded that high river discharge into the Atchafalaya Bay can lead to greater offshore transport (Thyng & Hetland, 2018; Zhang et al., 2012), similar to our current observation. In contrast, Barataria sector has limited inflow of direct freshwater, has a much steeper shelf slope (Bi et al., 2019), and is influenced by MSR plume driven by the Louisiana Coastal Current which is extremely responsive to wind forcing (Wiseman & Kelly, 1994).

Most studies of freshwater mixing over the Louisiana Shelf have dealt with freshwater plume pathways and thickness, in context of seasonal hypoxia and indicate that maximum offshore transport of the freshwater plumes in the mid Louisiana Shelf occur in mid-summer, depending on whether wind conditions are upwelling favorable (Thyng & Hetland, 2018; Zhang et al., 2012). Offshore transport is favored when the average wind direction is toward the southwest, while average wind oriented to the northwest is not associated with transport across the shelf (Thyng & Hetland, 2018; Zhang et al., 2012). During most of our study period, the average wind directions may not have been favorable for strong upwelling, suggesting a combination of turbulent mixing processes and nonlinear transport processes, such as momentum advection, was driving the offshore transport during this time. The offshore transport occurring during this study was strongly driven by freshwater discharge, with mixing rates decreasing from late spring to late summer, as river discharged

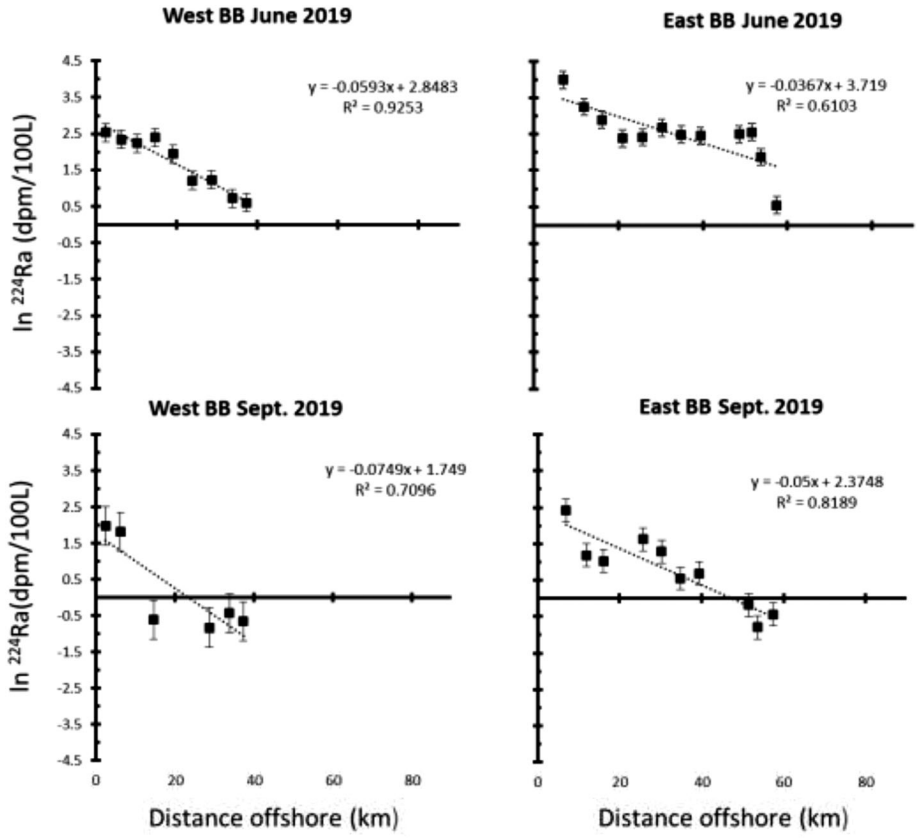

Figure 7. ^{224}Ra distribution along the two transects in Barataria Bay (BB) during June 2019 (upper panels) and September 2019 (lower panels).

decreased significantly. A regional oceanic modeling system (ROMS) setup validated for the entire NGOM region was utilized to simulate cross-shelf transport during out study period using point source dye inputs at river mouths (Shchepetkin & McWIlliams, 2005; Xue et al., 2016). Results from the ROMS simulation also indicate rapid cross-shelf transport of river derived material beyond the sampling domain during our sampling period (Figures S1 and S2).

A few studies have published horizontal mixing rates for the mid Louisiana Shelf. Brokaw et al. (2019) utilized satellite sea surface salinity and sea surface height to quantify low-salinity transport by the Loop Current System in the nGOM and estimated that average August offshore transport in the BB region to reach around 800 $m^2\ s^{-1}$. Ohlmann and Niiler (2005) used Lagrangian observations to characterize circulation over the nGOM shelf and estimated that the region near the WLD had a mixing rate of 640 $m^2\ s^{-1}$ between October 1993 and October 1994. Shelf water mixing rates (K_h) are influenced by a wide variety of environmental factors which generate water turbulence and therefore can be highly variable (Inman et al., 1971; Sippo et al., 2019). Given such wide variability in mixing rates as a function of freshwater discharge, currents, and prevailing wind strength and direction, these reported values can be considered similar to the mixing rates estimated in this current study. The only possible exception is the WLD west transect in June, where we report the highest rates for the region, which could be related to rivers being in flood stage during our sampling period (Figure 1). There are no prior estimates of radium-based mixing rates reported from our study region, and estimates from other coastal regions summarized in Table 2 are found to vary widely due to differences in their regional setting. Most of these reported studies are not from areas with strong river influence and hence are not directly comparable. The seasonal shifts in mixing rates in this study suggest variability in river discharge and other factors, such as bathymetry, play an important role in controlling mixing rates on the Louisiana Shelf, which would explain the large changes observed during this study period (Li & Cai, 2011).

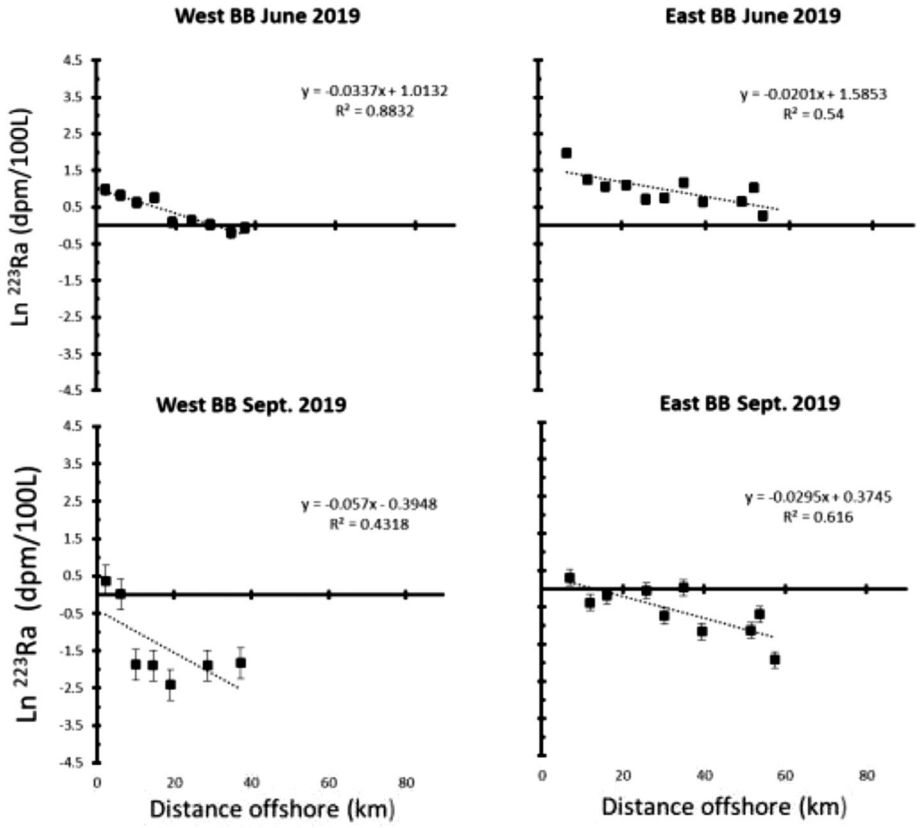

Figure 8. ^{223}Ra distribution along the two transects in Barataria Bay (BB) during June 2019 (upper panels) and September 2019 (lower panels).

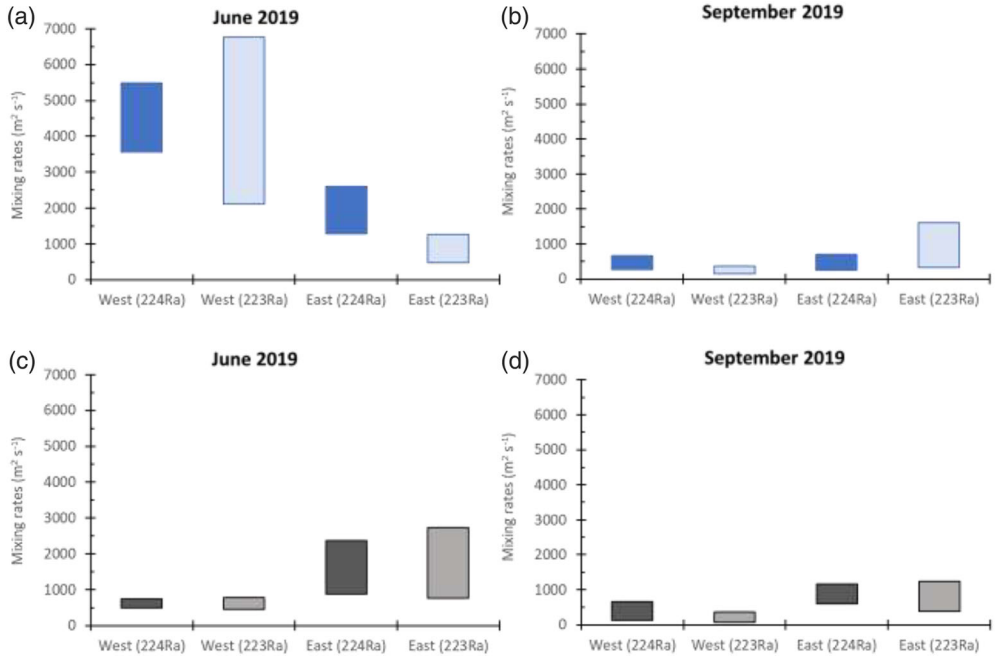

Figure 9. Estimated mixing rate range for the surface water within both the (a and b) WLD sector and (c and d) BB sector. Darker shaded bars indicate values estimated from ^{224}Ra values and lighter shaded bars indicate values estimated from ^{223}Ra values.

Table 2
^{224}Ra- and ^{223}Ra-Derived Mixing Rates From Published Literature

	Cross-shelf mixing rates	Environment	Location
Colbert and Hammond (2007)	1.4 m^2 s^{-1}	Tida- and current-influenced bay, little to no influence of seasonal river discharge	San Pedro Bay, California, USA
Sippo et al. (2019)	58–123 m^2 s^{-1}	Shallow shelf (8-m depth, 10-km offshore) and during no seasonal river discharge	Gulf of Carpentaria, Australia
Windom et al. (2006)	240–338 m^2 s^{-1}	Shelf off the coast of a barrier island	south Brazil
Sanders and Garvine (2001)	40–600 m^2 s^{-1}	Tidal and riverine discharge influenced bay with >25-m deep channel	Delaware Bay, USA
Dulaiova et al. (2009)	6.3×10^4 m^2 s^{-1}	Steep shelf and deep ocean (>1,000-m depth) near the Antarctic Circumpolar Current.	Elephant Island, Southern Drake Passage

4.2. Shelf Residence Time

To quantify the DIC transport across the shelf, a measure of residence time of the shelf water with respect to mixing is required. Residence time of water on the shelf is defined as the time required to remove the water from $1/e$ of the length of the shelf shown as follows:

$$L = (2\,K_h\,t)^{1/2} \tag{2}$$

where L is length of the shelf (WLD = 84 km; BB = 57 km), K_h is the mixing rate, and t is the residence time (Windom et al., 2006).

The average residence time of water in June 2019 in the WLD sector ranged from 7 to 28 and 4 to 68 days for ^{224}Ra and ^{223}Ra, respectively, and in the BB sector, it ranged from 6 to 36 days for ^{224}Ra and 5 to 38 days for ^{223}Ra, respectively (Figure 10). However, by September 2019, the average residence time of the WLD sector increased to 45–129 and 14–233 days for ^{224}Ra and ^{223}Ra, respectively, while that of BB sector increased to 15–81 and 11–149 days for ^{224}Ra and ^{223}Ra, respectively (Figure 10; Table 1). Moore and Krest (2004)

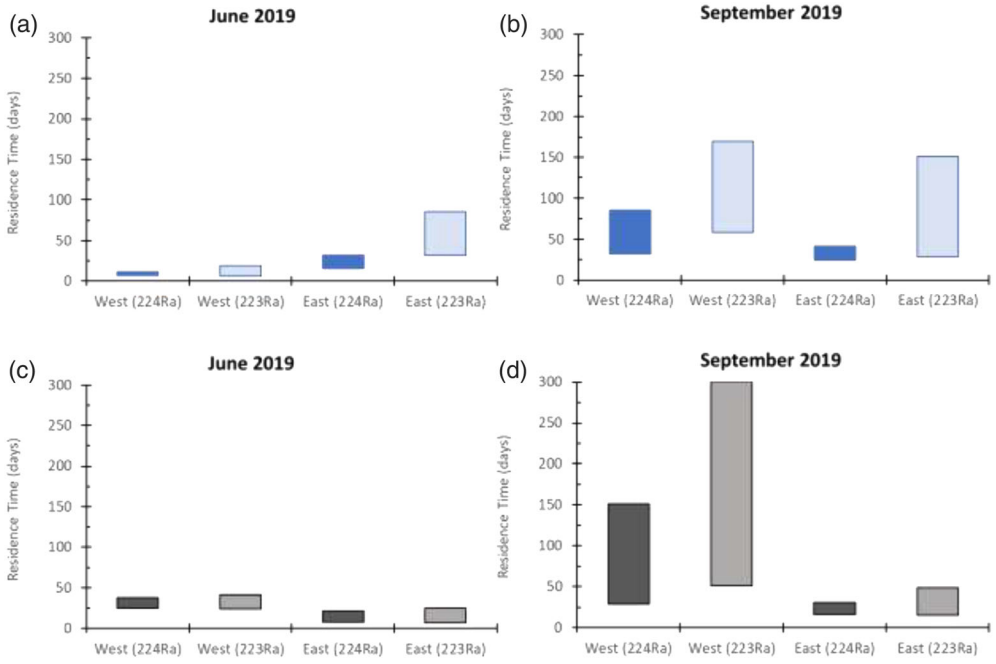

Figure 10. Estimated residence time range for surface water in both the (a and b) WLD sector and (c and d) BB sector. Darker shaded bars indicate values estimated from ^{224}Ra values and lighter shaded bars indicate values estimated from ^{223}Ra values.

calculated the $^{223}Ra/^{224}Ra$ age of the water mass with an S of 30 in the BB region to be between 8 and 21 days in May, which is similar to our current estimates.

Previous studies from this region have utilized two different approaches to estimating time scales of freshwater on the Louisiana Shelf. One approach is to estimate residence time or a transit time of freshwater. The second approach is to estimate the filling and flushing rate of freshwater on the shelf (Etter et al., 2004; Zhang et al., 2012). However, filling and flushing rates are not analogous to residence time estimates. Residence time is defined as the average time for water to escape the reservoir of the shelf, where flushing time is defined as the time required for freshwater discharge to equal the amount of freshwater originally present on the shelf (Sheldon & Alber, 2002). Therefore, we will only compare residence time estimates from our study to other studies which have used a residence/transit time approach in the Louisiana Shelf. Wiseman et al. (1997) utilized averaged time series data from 10 years of survey cruises in late July/early August on the Louisiana Shelf and estimated a 15-day lag of freshwater to a station located halfway between the WLD and BB sectors. Brokaw et al. (2019) estimated a K_h value of 800 $m^2\ s^{-1}$ in BB sector during August for 2013–2018. If we apply this K_h value to our BB study area parameters (Equation 2), it yields a residence time of 24 days, which is similar to our current estimates for late spring and early summer. Similarly, using the estimated K_h value of 640 $m^2\ s^{-1}$ in the WLD sector, reported for October 1993 near that region (Ohlmann & Niiler, 2005), results in a residence time of 64 days, which is similar to our September estimates (Table 1).

4.3. Transport of DIC

The surface DIC concentrations ranged between 1,765 and 2,390 μmol kg^{-1} similar to what has been previously reported from the region (Guo et al., 2012; Huang et al., 2018; Wang et al., 2013). The shelf DIC distribution indicates nonconservative behavior for both WLD and BB. The DIC distribution is indicative of significant biological control. Biogeochemical processes, such as photosynthesis, respiration, and air-sea CO_2 exchange can impact DIC. In the shallow shelf region, high concentrations of riverine nutrients stimulate intensive biological production throughout the water column, leading to the uptake of DIC and acts as the most important control on DIC distribution within the region. The biological uptake in this region is reported to be one of the highest in the world, ranging between 160 and 250 mmol $m^{-2}\ d^{-1}$ (Cai, 2003; Guo et al., 2012). Boundary current entrainment of shelf water DIC can also occur during summer, when Loop Current eddies approach and interact with the shelf processes, but it mostly occurs along the shelf break, further south of our study region (Wang et al., 2013).

The lateral transport of DIC in the surface-mixed layer can be estimated from the total DIC inventory in the water column and the corresponding radium-derived residence time (Table 1). The DIC inventory in the surface-mixed layer is calculated from the average DIC concentration within each sector and the volume of water for each study sector, based on the length and width of our study area boundaries (Figure 2) with a depth of 5 m, which is assumed to be the average surface-mixed layer depth. The water volume for each sector is estimated to be 13.86×10^9 m^3 in the WLD sector and 9.41×10^9 m^3 in the BB sector. In June 2019, the DIC transport from the WLD sector was estimated to be in the range of 0.86–3.69 $\times 10^9$ and 0.32–4.54 $\times 10^9$ mol d^{-1} based on ^{224}Ra and ^{223}Ra, respectively (Figure 11). The corresponding DIC transport from the BB sector was estimated to be between 0.51–2.42 $\times 10^9$ and 0.47–2.78 $\times 10^9$ mol d^{-1} based on ^{224}Ra and ^{223}Ra, respectively (Figure 11). Since transport is inversely related to residence time, the DIC transport of both sectors decreased with seasonal river decrease. In September 2019, the average DIC transport of the WLD transects ranged between 0.16–0.46 $\times 10^9$ and 0.09–1.05 $\times 10^9$ mol d^{-1} based on ^{224}Ra and ^{223}Ra, respectively, while the average DIC transport for the BB region ranged between 0.13–1.18 $\times 10^9$ and 0.06–1.26 $\times 10^9$ mol d^{-1} based on ^{224}Ra and ^{223}Ra, respectively (Figure 11). These estimates show that the WLD sector experienced a 5–8 times decrease in average DIC transport between June 2019 and September 2019, whereas the BB sector only experienced a 2–4 times decrease in average DIC transport between June 2019 and September 2019. This further highlights the importance of direct freshwater discharge from the AR into the bay.

The net DIC transport for both the WLD and BB sectors was greater during the period of high river discharge in late spring (June 2019) than during the low river discharge in late summer (September 2019). There is no significant difference in total DIC transport between the WLD sector and the BB sector in either season,

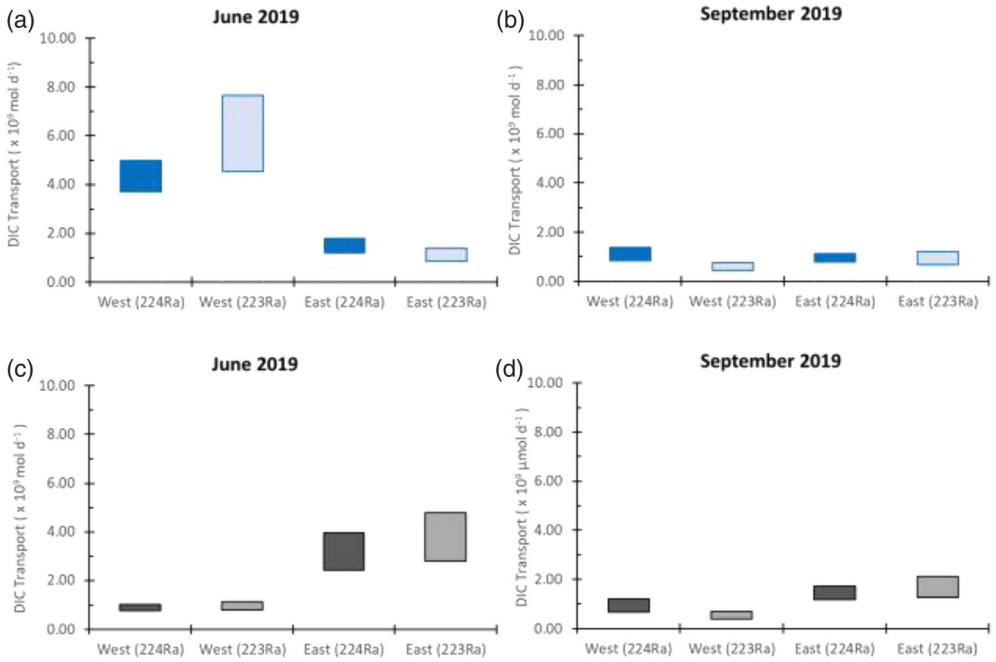

Figure 11. Estimated range of transport for DIC in the surface water within both the (a and b) WLD sector and (c and d) BB sector. Darker shaded bars indicate values estimated from ^{224}Ra values and lighter shaded bars indicate values estimated from ^{223}Ra values.

varying between 0.32×10^9 to 4.54×10^9 mol d^{-1} for June and 0.47×10^9 to 2.78×10^9 mol d^{-1} in September (t test, $p > 0.05$). However, we acknowledge that this is not a fair comparison because, volumetrically, the BB sector is approximately 68% that of the WLD sector when considering a uniform 5-m mixed layer depth. Thus, DIC transport per unit volume for each of the sectors can provide more comparable data. WLD transport decreased from 328–42 to 76–7 mmol m^{-3} d^{-1}, while BB transport decreased from 6,296–50 to 134–7 mmol m^{-3} d^{-1} in between June and September. To put this in perspective, the DIC contribution by the Loop Current in the nGOM is estimated to be 3.5 mmol m^{-3} d^{-1} (Wang et al., 2013). The Loop Current interacts directly with nearby shelves (Morey et al., 2003; Walker et al., 2005), suggesting that much of the DIC is ultimately supplied from the surrounding shelf, with the Louisiana Shelf playing a dominant role. It is estimated that DIC transport from all GOM shelves to Loop Current waters is ~ 3.30×10^{12} mol C yr^{-1} which is equivalent to ~9.04×10^9 mol C d^{-1}). Results from our study suggest that the Louisiana Shelf maybe a major contributor to DIC exported to offshore waters. If we extrapolate our DIC flux estimates for surface-mixed layer to the entire shelf up to the 35-m isobath, assuming the region between our WLD and BB sectors to behave similar to the BB sector, it translates to 1.54–20.19 $\times$ 10^9 mol C d^{-1} transported in June 2019 and 0.34–8.12 $\times$ 10^9 mol C d^{-1} transported in September 2019 across the shelf by the surface-mixed layer. In contrast, DIC transport across the entire East China Sea was estimated to be 0.20×10^{11} mol C d^{-1} (Tsunogai et al., 1997), while DIC transport across the entire South Atlantic Bight is estimated to be 0.59×10^9 mol C d^{-1} (Cai et al., 2003), suggesting the importance of DIC transport and its relation to shelf bathymetry and other environmental factors. These estimates provide a first-order idea of DIC transport within the shallowest sections of the shelf, which is often understudied in most regional studies, e.g., GOMECC carried out sampling at and beyond the 20-m isobath in this region (Wang et al., 2013). Moreover, these estimates will be highly variable, not only between seasons but also from year to year, as the river discharge is shown to play an important role in this transport.

Few studies have quantified the fluvial input of DIC into the Louisiana Shelf by the Mississippi-Atchafalaya River System. Cai et al. (2003) estimated the total DIC delivered from the Mississippi-Atchafalaya River System to the Louisiana shelf to be 1.8×10^{12} mol C yr^{-1}. More recent estimates indicate the net transport of carbon in the form of DIC to coastal waters from the MSR and AR to be 1.57×10^{12} mol C yr^{-1}

(Tian et al., 2015) and 4.46×10^{11} mol C yr^{-1} (DelDuco & Xu, 2019), respectively. It is difficult to make a direct comparison of these estimates of DIC river input with our current cross-shelf transport estimates. In 2019, the MSR stayed above flood stage for an unprecedented 226 days and had an annual discharge larger than the 10-year average (NOAA, 2019; USGS, 2016). For example, the average discharge rates during our study period were 31.5×10^3 and 10.5×10^3 m^3 s^{-1} in June and September, while the previously mentioned study (Cai, 2003) which estimated fluvial DIC input from the MSR experienced MSR discharge rates of 15.9×10^3 and 5.9×10^3 m^3 s^{-1} for the same months. The difference in river discharge rates between the Cai et al. (2003) study and our study is by a factor of 2. Nevertheless, if we translate the estimated annual river input of DIC to the shelf by Cai et al. (2003) to its average daily value, it comes to 5×10^9 mol C d^{-1} entering the Louisiana Shelf, which is lower by a factor of 2–3 than our current seasonal daily estimates of DIC transport across the shelf. The fluvial DIC input into the shelf during our study periods was likely higher than our estimated shelf transport rates, due to the uptake of DIC throughout the shelf region as a result of biological productivity (Xue et al., 2016).

5. Conclusions

Current rates of fluvial input of DIC into the coastal ocean are relatively well studied in the nGOM and, globally, rivers are estimated to contribute 0.38–2.6 Pg of DIC to world oceans (Lerman et al., 2007; Meybeck, 1982). However, estimates of fluvial-sourced DIC transport across shallow shelves in the nGOM and other river-dominated shelves throughout the globe are sparse. The present study indicates that approximately 1.54–20.19–10^9 mol C d^{-1} transported in June 2019 and 0.34–8.12×10^9 mol C d^{-1} in the form of DIC is exported across the surface-mixed layer of the Louisiana Shelf (up to 40-m isobath) during high and low river flow rates. More comprehensive seasonal studies coupled with biogeochemical modeling need to be carried out to provide a better understanding of annual-scale DIC transport. Lateral transport of DIC across the Louisiana Shelf is currently not well quantified (Coble et al., 2010), and current predictions suggest that Mississippi-Atchafalaya River discharge to coastal waters may increase by up to 59.8% by 2090 (Tao et al., 2014), which would impact the lateral export of both DIC and nutrients to the ocean interior dramatically in the future.

Data Availability Statement

The data set presented in this manuscript is publicly available on Louisiana State University, Center for Computation and Technology website at the following link (https://www.cct.lsu.edu/~zxue/JGR-2020-Maiti/JGR_data.pdf).

Acknowledgments

This work is primarily supported by NASA EPSCoR (award number NNH17ZHA002C) and Louisiana Board of Regents (award number NASA/LEQSF(2018-20)-Phase3-11). MMA and KM are also partly supported by NSF OCE 1756788. We are grateful for the assistance of the captain and crew of the *R/V Acadiana*. We thank Jocelyn Forsman, Patrick Owen Clower Bingqing Liu, Ivan Vargas, Le Zhang, Caitlin Neal, and Jill Broussard for help with sample collection. We would also like to thank Dr. Peter Santschi and another anonymous reviewer for their suggestions which greatly improved this manuscript.

References

Allen, Y. C., Couvillion, B. R., & Barras, J. A. (2012). Using multitemporal remote sensing imagery and inundation measures to improve land change estimates in coastal wetlands. *Estuaries and Coasts*, *35*(1), 190–200. https://doi.org/10.1007/s12237-011-9437-z

Bam, W., Maiti, K., & Ghaisas, N. A. (2016). ^{224}Ra: ^{228}Th disequilibrium in sediments as a tracer for solute transfer across the sediment-water Interface in Coastal Louisiana. In *American Geophysical Union, Ocean Sciences Meeting 2016, Abstract# MG33A-03*. New Orleans: AGU.

Barras, J. A., Beville, S., Britsch, D., Hartley, S., Hawes, S., Johnston, J., et al. (2003). *Historical and projected coastal Louisiana land changes: 1978–2050* (p. 39). Louisiana, US: United States Geological Survey.

Barras, J. A. (2006). *Land area change in coastal Louisiana after the 2005 hurricanes—A series of three maps: U.S. Geological Survey Open-File Report 06-1274*. Reston, VA: USGS.

Bi, W., Wang, J. J., Dodla, S. K., Gaston, L. A., & DeLaune, R. D. (2019). Lignin chemistry of wetland soil profiles in two contrasting basins of the Louisiana Gulf coast. *Organic Geochemistry*, *137*, 103,902. https://doi.org/10.1016/j.orggeochem.2019.103902

Bianchi, T. S., Filley, T., Dria, K., & Hatcher, P. G. (2004). Temporal variability in sources of dissolved organic carbon in the lower Mississippi River. *Geochimica et Cosmochimica Acta*, *68*(5), 959–967. https://doi.org/10.1016/j.gca.2003.07.011

Bianchi, T. S., Wysocki, L. A., Schreiner, K. M., Filley, T. R., Corbett, D. R., & Kolker, A. S. (2011). Sources of terrestrial organic carbon in the Mississippi plume region: Evidence for the importance of coastal marsh inputs. *Aquatic Geochemistry*, *17*(4–5), 431–456. https://doi.org/10.1007/s10498-010-9110-3

Bianchi, T. S., Wysocki, L. A., Stewart, M., Filley, T. R., & McKee, B. A. (2007). Temporal variability in terrestrially-derived sources of particulate organic carbon in the lower Mississippi River and its upper tributaries. *Geochimica et Cosmochimica Acta*, *71*(18), 4425–4437. https://doi.org/10.1016/j.gca.2007.07.011

Blum, M. D., & Roberts, H. H. (2009). Drowning of the Mississippi Delta due to insufficient sediment supply and global sea-level rise. *Nature Geoscience*, *2*(7), 488–491. https://doi.org/10.1038/ngeo553

Brokaw, R. J., Subrahmanyam, B., & Morey, S. L. (2019). Loop current and eddy-driven salinity variability in the Gulf of Mexico. *Geophysical Research Letters*, *46*, 5978–5986. https://doi.org/10.1029/2019GL082931

Burt, W. J., Thomas, H., & Auclair, J. P. (2013). Short-lived radium isotopes on the Scotian Shelf: Unique distribution and tracers of cross-shelf CO_2 and nutrient transport. *Marine Chemistry*, *156*, 120–129. https://doi.org/10.1016/j.marchem.2013.05.007

Cai, W. J. (2003). Riverine inorganic carbon flux and rate of biological uptake in the Mississippi River plume. *Geophysical Research Letters*, *30*(2), 1032. https://doi.org/10.1029/2002GL016312

Cai, W. J., Hu, X., Huang, W. J., Murrell, M. C., Lehrter, J. C., Lohrenz, S. E., et al. (2011). Acidification of subsurface coastal waters enhanced by eutrophication. *Nature Geoscience*, *4*(11), 766. https://doi.org/10.1038/ngeo1297

Cai, W. J., Wang, Z. A., & Wang, Y. (2003). The role of marsh-dominated heterotrophic continental margins in transport of CO_2 between the atmosphere, the land-sea interface and the ocean. *Geophysical Research Letters*, *30*(16), 1849. https://doi.org/10.1029/2003GL017633

Cai, Y. H., Guo, L. D., Wang, X. R., & Aiken, G. (2015). Abundance, stable isotopic composition, and export fluxes of DOC, POC, and DIC from the lower Mississippi River during 2006–2008. *Journal of Geophysical Research: Biogeosciences*, *120*, 2273–2288. https://doi.org/10.1002/2015JG003139

Chen, W. F., Liu, Q. A., Huh, C. A., Dai, M. H., & Miao, Y. C. (2010). Signature of the Mekong River plume in the western South China Sea revealed by radium isotopes. *Journal of Geophysical Research*, *115*, C12002. https://doi.org/10.1029/2010JC006460

Coble, P. G., Robbins, L. L., Daly, K. L., Cai, W. J., Fennel, K., & Lorenz, S. E. (2010). A preliminary carbon budget for the Gulf of Mexico. *Ocean Carbon and Biogeochemistry Newsletter*, *3*(3), 1.

Colbert, S. L., & Hammond, D. E. (2007). Temporal and spatial variability of radium in the coastal ocean and its impact on computation of nearshore cross-shelf mixing rates. *Continental Shelf Research*, *27*(10–11), 1477–1500. https://doi.org/10.1016/j.csr.2007.01.003

Couvillion, B. R. (2011). Land change in Coastal Louisiana from 1932 to 2010, scale 1:265,000. In *U.S. Geological Survey Scientific Investigations Map 3164* (p. 12). Reston, VA: USGS.

Couvillion, B. R., Beck, H., Schoolmaster, D., & Fischer, M. M. (2017). *Land area change in Coastal Louisiana (1932 to 2016), U.S. Geological Survey Scientific Investigations Map 3381* (p. 16). Reston VA: USGS.

DelDuco, E. M., & Xu, Y. J. (2019). Dissolved carbon transport and processing in North America's largest swamp river entering the northern Gulf of Mexico. *Watermark*, *11*(7), 1395. https://doi.org/10.3390/w11071395

Dickson, A. G. (2010). Standards for ocean measurements. *Oceanography*, *23*(3), 34–47. https://doi.org/10.5670/oceanog.2010.22

Dulaiova, H., Ardelan, M. V., Henderson, P. B., & Charette, M. A. (2009). Shelf-derived iron inputs drive biological productivity in the southern Drake Passage. *Global Biogeochemical Cycles*, *23*, 14. https://doi.org/10.1029/2008GB003406

Etter, P. C., Howard, M. K., & Cochrane, J. D. (2004). Heat and freshwater budgets of the Texas-Louisiana Shelf. *Journal of Geophysical Research*, *109*, C02024. https://doi.org/10.1029/2003JC001820

Fitzgerald, D. M., Kulp, M., Penland, S., Flocks, J., & Kindinger, J. (2004). Morphologic and stratigraphic evolution of muddy ebb-tidal deltas along a subsiding coast: Barataria Bay, Mississippi River Delta. *Sedimentology*, *51*(6), 1157–1178. https://doi.org/10.1111/j.1365-3091.2004.00663.x

Guo, X., Cai, W. J., Huang, W. J., Wang, Y., Chen, F., Murrell, M. C., et al. (2012). Carbon dynamics and community production in the Mississippi River plume. *Limnology and Oceanography*, *57*(1), 1–17. https://doi.org/10.4319/lo.2012.57.1.0001

Holm, G. O., & Sasser, C. E. (2001). Differential salinity response between two Mississippi River subdeltas: Implications for changes in plant composition. *Estuaries*, *24*(1), 78–89. https://doi.org/10.2307/1352815

Hopkinson, C. S., Cai, W. J., & Hu, X. P. (2012). Carbon sequestration in wetland dominated coastal systems—A global sink of rapidly diminishing magnitude. *Current Opinion in Environmental Sustainability*, *4*(2), 186–194. https://doi.org/10.1016/j.cosust.2012.03.005

Huang, T. H., Lun, Z. X., Wu, C. R., & Chen, C. T. A. (2018). Interannual carbon and nutrient fluxes in southeastern Taiwan Strait. *Sustainability*, *10*(2), 15. https://doi.org/10.3390/su10020372

Inman, D. L., Tait, R. J., & Nordstrom, C. E. (1971). Mixing in the surf zone. *Journal of Geophysical Research*, *76*(15), 3493–3514. https://doi.org/10.1029/JC076i015p03493

Intergovernmental Panel on Climate Change (2014). *Climate change 2013: The physical science basis: Working group I contribution to the Fifth Assessment Report of the Intergovernmental Panel on Climate Change*. Cambridge: Cambridge University Press. https://doi.org/10.1017/CBO9781107415324

Kolker, A. S., Allison, M. A., & Hameed, S. (2011). An evaluation of subsidence rates and sea-level variability in the northern Gulf of Mexico. *Geophysical Research Letters*, *38*, L21404. https://doi.org/10.1029/2011GL049458

Krest, J. M., & Moore, W. S. (1999). ^{226}Ra and ^{228}Ra in the mixing zones of the Mississippi and Atchafalaya Rivers: indicators of groundwater input. *Marine Chemistry*, *64*(3), 129–152. https://doi.org/10.1016/S0304-4203(98)00070-X

Lerman, A., Wu, L., & Mackenzie, F. T. (2007). CO_2 and H_2SO_4 consumption in weathering and material transport to the ocean, and their role in the global carbon balance. *Marine Chemistry*, *106*(1–2), 326–350. https://doi.org/10.1016/j.marchem.2006.04.004

Li, C. Y., & Cai, W. J. (2011). On the calculation of eddy diffusivity in the shelf water from radium isotopes: High sensitivity to advection. *Journal of Marine Systems*, *86*(1–2), 28–33. https://doi.org/10.1016/j.jmarsys.2011.01.003

Meybeck, M. (1982). Carbon, nitrogen, and phosphorus transport by world rivers. *American Journal of Science*, *282*, 401–450. https://doi.org/10.2475/ajs.282.4.401

Moore, W. S. (1976). Sampling ^{228}Ra in the deep ocean. *Deep Sea Research and Oceanographic Abstracts*, *23*(7), 647–651. https://doi.org/10.1016/0011-7471(76)90007-3

Moore, W. S. (2000). Ages of continental shelf waters determined from ^{223}Ra and ^{224}Ra. *Journal of Geophysical Research*, *105*(C9), 22,117–22,122. https://doi.org/10.1029/1999JC000289

Moore, W. S., & Arnold, R. (1996). Measurement of ^{223}Ra and ^{224}Ra in coastal waters using a delayed coincidence counter. *Journal of Geophysical Research*, *101*(C1), 1321–1329. https://doi.org/10.1029/95JC03139

Moore, W. S., & Krest, J. (2004). Distribution of ^{223}Ra and ^{224}Ra in the plumes of the Mississippi and Atchafalaya rivers and the Gulf of Mexico. *Marine Chemistry*, *86*(3–4), 105–119. https://doi.org/10.1016/j.marchem.2003.10.001

Morey, S. L., Martin, P. J., O'Brien, J. J., Wallcraft, A. A., & Zavala-Hidalgo, J. (2003). Export pathways for river discharged fresh water in the northern Gulf of Mexico. *Journal of Geophysical Research*, *108*, 3303. https://doi.org/10.1029/2002JC001674

National Data Buoy Center (1971). Meteorological and oceanographic data collected from the National Data Buoy Center Coastal-Marine Automated Network (C-MAN) and moored (weather) buoys. Station GISL1-8761724 - Grand Isle, LA] NOAA National Centers for Environmental Information. Dataset. https://accession.nodc.noaa.gov/NDBC-CMANWx. Accessed [04/16/2020].

Ohlmann, J. C., & Niiler, P. P. (2005). Circulation over the continental shelf in the northern Gulf of Mexico. *Progress in Oceanography*, *64*(1), 45–81. https://doi.org/10.1016/j.pocean.2005.02.001

Rosen, T., & Xu, Y. J. (2013). Recent decadal growth of the Atchafalaya River Delta complex: Effects of variable riverine sediment input and vegetation succession. *Geomorphology*, *194*, 108–120. https://doi.org/10.1016/j.geomorph.2013.04.020

Sanders, T. M., & Garvine, R. W. (2001). Fresh water delivery to the continental shelf and subsequent mixing: An observational study. *Journal of Geophysical Research*, *106*(C11), 27,087–27,101. https://doi.org/10.1029/2001JC000802

Schuerch, M., Spencer, T., Temmerman, S., Kirwan, M. L., Wolff, C., Lincke, D., et al. (2018). Future response of global coastal wetlands to sea-level rise. *Nature*, *561*(7722), 231–234. https://doi.org/10.1038/s41586-018-0476-5

Second New Orleans District, U.S. Army Corps of Engineers, 1938 *Second New Orleans District, U.S. Army Corps of Engineers Wax Lake Outlet, Constructed by the Corps of Engineers, U.S. Army*. (p. 14 and appendices)

Shchepetkin, A. F., & McWIlliams, J. C. (2005). The regional oceanic modeling system (ROMS): A split-explicit, free-surface, topography-following coordinate oceanic model. *Ocean Model*, *9*(4), 347–404. https://doi.org/10.1016/j.ocemod.2004.08.002

Sheldon, J. E., & Alber, M. (2002). A comparison of residence time calculations using simple compartment models of the Altamaha River estuary, Georgia. *Estuaries*, *25*(6B), 1304–1317. https://doi.org/10.1007/BF02692226

Sippo, J. Z., Maher, D. T., Schulz, K. G., Sanders, C. J., McMahon, A., Tucker, J., & Santos, I. R. (2019). Carbon outwelling across the shelf following a massive mangrove dieback in Australia: Insights from radium isotopes. *Geochimica et Cosmochimica Acta*, *253*, 142–158. https://doi.org/10.1016/j.gca.2019.03.003

Spencer, T., Schuerch, M., Nicholls, R. J., Hinkel, J., Lincke, D., Vafeidis, A. T., et al. (2016). Global coastal wetland change under sea-level rise and related stresses: The DIVA wetland change model. *Global and Planetary Change*, *139*, 15–30. https://doi.org/10.1016/j.gloplacha.2015.12.018

Suchet, P. A., Probst, J. L., & Ludwig, W. (2003). Worldwide distribution of continental rock lithology: Implications for the atmospheric/soil CO_2 uptake by continental weathering and alkalinity river transport to the oceans. *Global Biogeochemical Cycles*, *17*(2). https://doi.org/10.1029/2002GB001891

Tao, B., Tian, H., Ren, W., Yang, J., Yang, Q., He, R., et al. (2014). Increasing Mississippi River discharge throughout the 21st century influenced by changes in climate, land use, and atmospheric CO_2. *Geophysical Research Letters*, *41*, 4978–4986. https://doi.org/10.1002/2014GL060361

Thyng, K. M., & Hetland, R. D. (2018). Seasonal and interannual cross-shelf transport over the Texas and Louisiana continental shelf. *Continental Shelf Research*, *160*, 23–35. https://doi.org/10.1016/j.csr.2018.03.006

Tian, H. Q., Ren, W., Yang, J., Tao, B., Cai, W. J., Lohrenz, S. E., et al. (2015). Climate extremes dominating seasonal and interannual variations in carbon export from the Mississippi River Basin. *Global Biogeochemical Cycles*, *29*, 1333–1347. https://doi.org/10.1002/2014GB005068

Tsunogai, S., Watanabe, S., Nakamura, J., Ono, T., & Sato, T. (1997). A preliminary study of carbon system in the East China Sea. *Journal of Oceanography*, *53*(1), 9–17. https://doi.org/10.1007/BF02700744

U.S. Geological Survey (2016). *National water information system data available on the World Wide Web (USGS Water Data for the Nation)*. accessed [March 27, 2020], Retrieved from http://waterdata.usgs.gov/nwis/

US Department of Commerce, and NOAA (2019). Mississippi River flood history 1543–present. In *National Weather Service*. US Dept of Commerce, National Oceanic and Atmospheric Administration, National Weather Service: NOAA's National Weather Service. 10 Aug. 2019, www.weather.gov/lix/ms_flood_history

Walker, N. D., Wiseman, W. J. Jr., Rouse, L. J. Jr., & Babin, A. (2005). Effects of river discharge, wind stress, and slope eddies on circulation and the satellite-observed structure of the Mississippi River plume. *Journal of Coastal Research*, *2005*(216), 1228–1244. https://doi.org/10.2112/04-0347.1

Wang, H. Q., Steyer, G. D., Couvillion, B. R., Beck, H. J., Rybczyk, J. M., Rivera-Monroy, V. H., et al. (2017). Predicting landscape effects of Mississippi River diversions on soil organic carbon sequestration. *Ecosphere*, *8*(11), 15. https://doi.org/10.1002/ecs2.1984

Wang, Z. H. A., Wanninkhof, R., Cai, W. J., Byrne, R. H., Hu, X. P., Peng, T. H., & Huang, W.-J. (2013). The marine inorganic carbon system along the Gulf of Mexico and Atlantic coasts of the United States: Insights from a transregional coastal carbon study. *Limnology and Oceanography*, *58*(1), 325–342. https://doi.org/10.4319/lo.2013.58.1.0325

Windom, H. L., Moore, W. S., Niencheski, L. F. H., & Jahnke, R. A. (2006). Submarine groundwater discharge: A large, previously unrecognized source of dissolved iron to the South Atlantic Ocean. *Marine Chemistry*, *102*(3–4), 252–266. https://doi.org/10.1016/j.marchem.2006.06.016

Wiseman, W. J., & Kelly, F. J. (1994). Salinity variability within the Louisiana Coastal Current during the 1982 flood season. *Estuaries*, *17*(4), 732–739. https://doi.org/10.2307/1352743

Wiseman, W. J., Rabalais, N. N., Turner, R. E., Dinnel, S. P., & MacNaughton, A. (1997). Seasonal and interannual variability within the Louisiana Coastal Current: Stratification and hypoxia. *Journal of Marine Systems*, *12*(1–4), 237–248. https://doi.org/10.1016/S0924-7963(96)00100-5

Xue, Z., He, R., Fennel, K., Cai, W. J., Lohrenz, S., Huang, W. J., et al. (2016). Modeling pCO_2 variability in the Gulf of Mexico. *Biogeosciences*, *13*, 4359. https://doi.org/10.5194/bgd-11-12673-2014

Zhang, X. Q., Hetland, R. D., Marta-Almeida, M., & DiMarco, S. F. (2012). A numerical investigation of the Mississippi and Atchafalaya freshwater transport, filling and flushing times on the Texas-Louisiana Shelf. *Journal of Geophysical Research*, *117*, C11009. https://doi.org/10.1029/2012JC008108